

Attenuation of voltage sags effects and dynamic performance improvement of a multi-motor system

Bensaid Mounir, Abdellfattah Ba-Razzouk, Mustapha Elharoussi, Bouchaib Rached

Systems Analysis and Information Processing (ASTI) Team, Mathematics, Computer and Engineering Sciences Laboratory (MISI), Hassan First University of Settat, Settat, Morocco

Article Info

Article history:

Received Sep 13, 2021

Revised Mar 20, 2022

Accepted Apr 7, 2022

Keywords:

Backstepping

Induction motor

Indirect rotor field-oriented control

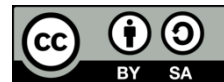
Multi-motors system

Voltage sag

ABSTRACT

In many continuous manufacturing processes such as paper, textile, winding and plastic extrusion, electric drives are frequently required to work in synchronization, often with high tolerances to ensure uniform product quality and avoid failure of the product. In a multi-motor system (MMS), voltage dips are the most common cause of the motor stoppage, and the transient loss of synchronism between motors can result in a complete system shutdown. This paper proposes a multi-motor system controlled by a Backstepping strategy to ensure servo-control and synchronization of induction motors. This technique includes indirect rotor field-oriented control (IRFOC), linear speed control, and mechanical tension control, of induction motors. Investigations of symmetrical voltage sag effects on speed, torque, and mechanical tension are also carried out. Simulation results obtained using Matlab®/Simulink™/SimPowerSystems® are presented to demonstrate the efficiency of the proposed control strategy.

This is an open access article under the [CC BY-SA](https://creativecommons.org/licenses/by-sa/4.0/) license.



Corresponding Author:

Mounir BENSaid

Systems Analysis and Information Processing (ASTI) Team, Mathematics, Computer and Engineering Sciences Laboratory (MISI), Hassan First University of Settat, Settat, Morocco

Email: bensaidmounir.eae@gmail.com

NOMENCLATURE

IM_i ($i=1,2$)	: Induction motor i
V_i ($i=1,2$)	: Linear velocity of motor i
f_i ($i=1,2$)	: Coefficient of viscous friction of the motor i
J_i ($i=1,2$)	: Inertia moment of the motor i
R_i ($i=1,2$)	: Ray of the roller i
L_b	: Enchainment length
ω_{mi} ($i=1,2$)	: Rotation speed of the motor i
T_{loadi} ($i=1,2$)	: Resistive torque
T_{ei} ($i=1,2$)	: Electromagnetic couple
$\phi_{r di}$ and $\phi_{r qi}$: Rotor fluxes following the axes direct and into quadratic
$i_{s di}$ and $i_{s qi}$: Stator currents following the axes direct and into quadratic
$u_{s di}$ and $u_{s qi}$: Stator voltage following the axes direct and into quadratic

1. INTRODUCTION

In many continuous manufacturing processes such as paper, textile, winding and plastic extrusion, electric drives are frequently required to work in synchronization, often with high tolerances to ensure uniform product quality and avoid failure of the product [1]. The correct functionality of these systems requires control

of the mechanical tension and the speed of the winding or material transport, which requires maintaining synchronization between the motor [2], [3].

Voltage sags, as defined by the IEEE-1159 standard, are brief drops in rms voltage to between 0.1 and 0.9 pu for durations ranging from 0.5 to 1 minute [4]. Short-circuiting faults, such as single line-to-ground faults in a power system, and the start-up of large rating motors are the most common causes of voltage dips. Such issues cause significant disruptions in motor speed and material mechanical tension, resulting in massive financial production losses [5].

The main effects of voltage dips include: the decrease in dc link voltage which degrades the functionality of the multi-motor system (MMS) and may cause it to shut down through the protection systems, the high current at the end of the dip when the dc link voltage has been reduced during the dip, which can cause significant damage to the system, and in general, sudden variations of the dc link voltage that affect the synchronism of the controllers and that can damage or destroy the various components of the system [5]. This problem has piqued the interest of many researchers, who are currently investigating it. Many solutions have been considered and proposed, many of which involve modifications to the traditional topology of multi-motor systems and/or incur significant costs. Mechanical or electrical auxiliary energy storage units [6], [7], unified power quality controller (UPQC) [8], [9], the application of converters with inductive elements, such as autotransformers, static power compensators (STATCOM) [10], static voltage regulator (SVR), dynamic voltage restorer (DVR) [11], [12] and energy storage devices including superconducting magnetic energy storage (SMES) [13]. These solutions, however, are still general in nature and have not been applied in multi-motor configurations.

Blaschke's field-oriented control is one of the most widely used induction motor control strategies. However, this technique is extremely sensitive to parameter changes. Sliding mode control [14], [15], for example, is one of many modified nonlinear state feedback systems. Input-output linearization control [16], passivity-based control [17], and backstepping control [18], have been presented in the literature to overcome this restriction. Backstepping control law is derived from a Lyapunov function to ensure system input-output stability and provides good performance in both steady state and transient operations, even in the presence of parameter variations and load torque disturbances [19]. In this paper, a Backstepping induction motor speed and mechanical tension controller for a multi-motor system is developed and will be evaluated by a simulation in the presence of voltage sags.

This paper is organized as follows. The nonlinear model of a simple winder system powered by two 4 kW three-phase induction motors is presented in section 2. Section 3 details the principles and design of the proposed backstepping controller. Section 4 gives the simulation results of the proposed strategy, obtained using Matlab®/Simulink™/SimPowerSystems®/RT-Lab®. Finally, section 5 summarizes the main contributions and describes some additional research avenues.

2. MODELING OF THE STUDIED SYSTEM

The control of multi-motor systems in the presence of voltage sags will be evaluated by simulation. Figures 1 and 2 shows a drive system consisting of two three-phase motors with a common DC bus, which are mechanically coupled by an elastic band with an adjustable mechanical tension. Motor IM1 performs unwinding whereas motor IM2 performs winding. This system is composed of two different parts, the mechanical part and the electrical part [5], [20], [21].

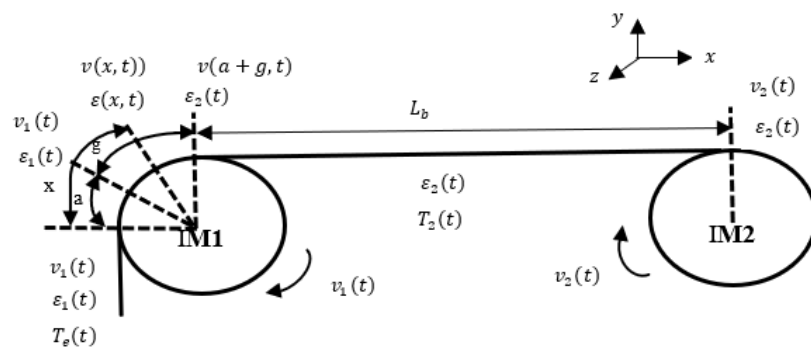


Figure 1. Web tension on the roll

2.1. Electric drive

The model consists of two three-phase asynchronous motors; the drives are connected to DC bus, to which an adjustable capacitor bank is connected, allowing the energy, allowing the energy characteristics of the system to be modified, Figure 2. The motors (IM1, IM2) are powered by PWM inverters in order to vary the speed. The electrical converter that connects the input power to the DC bus is a three-phase rectifier bridge with diodes. A model based on motor equivalent circuit equations is usually sufficient to synthesize the control law [22]–[25]. In the d-q synchronously rotating frame, the electrical dynamic model of a three-phase Y-connected induction motor IMi can be expressed as:

$$\begin{cases} \frac{d\omega_{mi}}{dt} = \mu_i \varphi_{r di} i_{sqi} - \frac{T_{loadi}}{J_i} \\ \frac{d\varphi_{r di}}{dt} = -a_i R_{ri} \varphi_{r di} + a_i R_{ri} L_{mi} i_{sdi} \\ \frac{di_{sdi}}{dt} = \psi_{1i} + \frac{1}{\sigma_i L_{si}} u_{sdi} \\ \frac{di_{sqi}}{dt} = \psi_{2i} + \frac{1}{\sigma_i L_{si}} u_{sqi} \\ \frac{d\theta_{si}}{dt} = p\omega_{mi} + a_i R_{ri} L_{mi} \frac{i_{sqi}}{\varphi_{r di}} \end{cases} \quad (1)$$

With:

$$\begin{aligned} \psi_{1i} &= -\eta_{1i} i_{sdi} + p\omega_{mi} i_{sqi} + R_{ri} \left(-\eta_{2i} i_{sdi} + a_i b_i \varphi_{r di} + a_i L_{mi} \frac{i_{sqi}^2}{\varphi_{r di}} \right) \\ \psi_{2i} &= -\eta_{1i} i_{sqi} + b_i p\omega_{mi} \varphi_{r di} - p\omega_{mi} i_{sdi} - R_{ri} \left(-\eta_{2i} i_{sdi} + a_i L_{mi} \frac{i_{sqi} i_{sdi}}{\varphi_{r di}} \right) \\ \mu_i &= \frac{3pL_{mi}}{2J_i L_{ri}} ; \eta_{1i} = \frac{R_{si}}{\sigma_i L_{ri}} ; \eta_{2i} = \frac{L_{mi}^2}{\sigma_i L_{si} L_{ri}^2} ; a_i = \frac{1}{L_{ri}} ; b_i = \frac{L_{mi}}{\sigma_i L_{si} L_{ri}} \end{aligned}$$

The electromagnetic torque is given by (2).

$$T_{ei} = p \cdot \frac{M_{sri}}{L_{ri}} \cdot \varphi_{ri} \cdot i_{sqi} \quad (2)$$

Where the parameters of the induction motor are defined in Table 1 and the different physical variables are defined in the nomenclature.

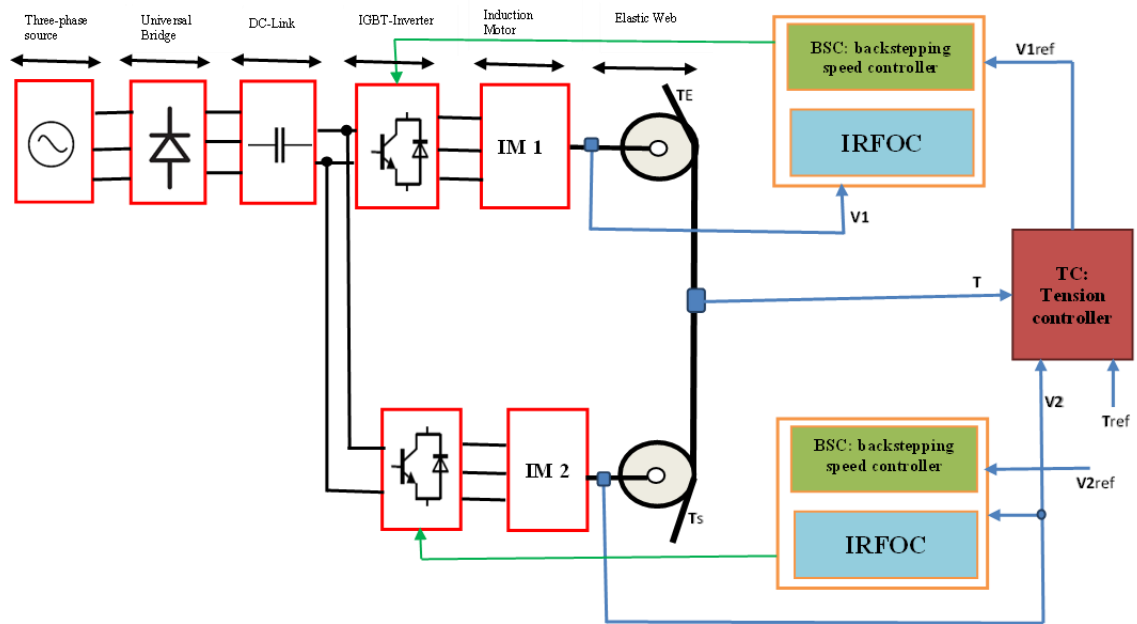


Figure 2. Multi-motor web coupled structure control

2.2. Electrical and mechanical models

The web-transport system's model is based on three laws, Hooke's law, Coulomb's law and mass conservation law, which enable to calculate the web tension between the two rolls [5], [26]. Where the dynamical equation of mechanical web tension T in (3) is a function of induction motor linear speeds V_1 and V_2 and web length L_b .

$$L_b \frac{dT_2}{dt} \cong ES(V_2 - V_1) + T_1 V_1 - T_2(2V_1 - V_2) \quad (3)$$

Model of the mechanical of the system is given by,

$$\begin{aligned} \frac{d(J_1(t)\Omega_1)}{dt} &= R_1(t)T + T_{m1} - f_1(t)\Omega_1 \\ L_b \frac{dT}{dt} &= V_2(ES + T) - V_1(ES - T_E + 2T) \\ \frac{d(J_2(t)\Omega_2)}{dt} &= -R_2(t)T + T_{m2} - f_2(t)\Omega_2 \end{aligned} \quad (4)$$

Using this equation, it is easy to see that the tension force in the section studied (T) is produced by the coupling of several variables in the system. Indeed, it depends on the length (L_b), the band section (S), the Young modulus (E) of the band and the rollers radius R_1 and R_2 .

2.3. Control structure

The strategy control structure shown in Figures 2 and 3 are implemented using backstepping speed controllers (BSC) combined with IRFOC. The mechanical tension control can be realized with a classical controller PI this controller generates the speed reference for IM1 in a cascade control loop structure [5], [19], [23], [27].

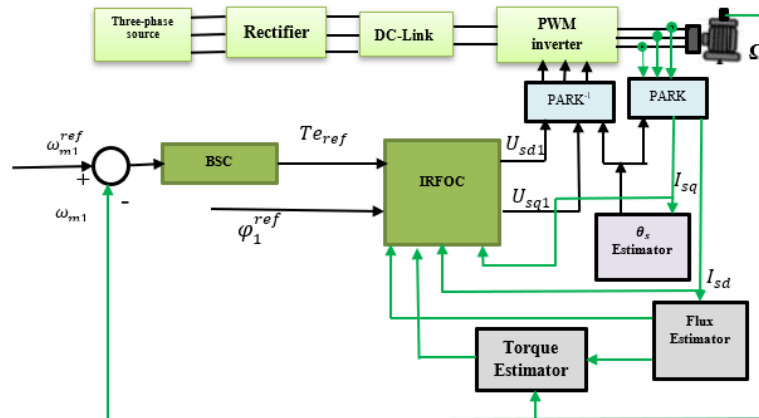


Figure 3. Block diagram of backstepping control scheme-based induction motor drive

Backstepping control strategy development steps are:

Step 1: Calculating stator currents and torque references:

Let us introduce the rotor speed and the flux tracking errors with their derivatives:

$$\begin{cases} e_1 = \omega_{mi}^{ref} - \omega_{mi} \\ e_3 = \varphi_i^{ref} - \varphi_i \end{cases} \quad (5)$$

So, the dynamic equations of the errors are:

$$\begin{cases} \frac{de_1}{dt} = \frac{d\omega_{mi}^{ref}}{dt} - \mu_i \varphi_{rdi} \dot{i}_{sqi} - \frac{T_{loadi}}{J_i} \\ \frac{de_3}{dt} = \frac{d\varphi_i^{ref}}{dt} + a_i R_{ri} \varphi_{rdi} - a_i R_{ri} L_{mi} \dot{i}_{sdi} \end{cases} \quad (6)$$

To check, consider the tracking performances to be the first Lyapunov candidate function V_1 associated with rotor flux and speed errors, such as:

$$V_1 = \frac{1}{2} e_1^2 + \frac{1}{2} e_3^2 \quad (7)$$

Using (5), the derivative of (6) is written as:

$$\begin{aligned} \frac{dV_1}{dt} &= \frac{de_1}{dt} \cdot e_1 + \frac{de_3}{dt} \cdot e_3 \\ &= \left(\frac{d\omega_{mi}^{ref}}{dt} - \mu_i \varphi_{rdi} \dot{i}_{sqi} - \frac{T_{loadi}}{J_i} \right) \cdot e_1 + \left(\frac{d\varphi_i^{ref}}{dt} + a_i R_{ri} \varphi_{rdi} - a_i R_{ri} L_{mi} \dot{i}_{sdi} \right) \cdot e_3 \\ &= -k_1 e_1^2 - k_3 e_3^2 + \left(k_1 e_1 + \frac{d\omega_{mi}^{ref}}{dt} - \mu_i \varphi_{rdi} \dot{i}_{sqi} - \frac{T_{loadi}}{J_i} \right) \cdot e_1 + \\ &\quad \left(k_3 e_3 + \frac{d\varphi_i^{ref}}{dt} + a_i R_{ri} \varphi_{rdi} - a_i R_{ri} L_{mi} \dot{i}_{sdi} \right) \cdot e_3 \end{aligned} \quad (8)$$

This can be rewritten as:

$$\frac{dV_1}{dt} = -k_1 e_1^2 - k_3 e_3^2 \leq 0 \quad (9)$$

In order to ensure stable tracking, k_1 and k_3 should be positive parameters. This results in:

$$\begin{cases} \frac{de_1}{dt} = \frac{d\omega_{mi}^{ref}}{dt} - \frac{d\omega_{mi}}{dt} = -k_1 e_1 \\ \frac{de_3}{dt} = \frac{d\varphi_i^{ref}}{dt} - \frac{d\varphi_i}{dt} = -k_3 e_3 \end{cases} \quad (10)$$

The stator current and torque references can then be deduced as:

$$\begin{cases} i_{isq}^{ref} = \frac{1}{\mu_i \varphi_{rdi}} \left(k_1 e_1 + \frac{d\omega_{mi}^{ref}}{dt} + \frac{T_{loadi}}{J_i} \right) \\ i_{isd}^{ref} = \frac{1}{a_i R_{ri} L_{mi}} \left(k_3 e_3 + \frac{d\varphi_i^{ref}}{dt} + a_i R_{ri} \varphi_{rdi} \right) \end{cases} \quad (11)$$

$$T_{m_ref} = p \frac{M_{sr}}{L_r} \varphi_r i_{sq_ref} \quad (12)$$

Step 2: Set-point computation of stator voltages

This step proposes a method for obtaining the current references generated by the first step. Consider the following current errors:

$$\begin{cases} e_2 = i_{isq}^{ref} - i_{sq} = \frac{1}{\mu_i \varphi_{rdi}} \left(k_1 e_1 + \frac{d\omega_{mi}^{ref}}{dt} + \frac{T_{loadi}}{J_i} \right) - i_{sq} \\ e_4 = i_{isd}^{ref} - i_{isd} = \frac{1}{a_i R_{ri} L_{mi}} \left(k_3 e_3 + \frac{d\varphi_i^{ref}}{dt} + a_i R_{ri} \varphi_{rdi} \right) - i_{isd} \end{cases} \quad (13)$$

As a result, the error (12) can be written as:

$$\begin{cases} \frac{de_1}{dt} = -k_1 e_1 + \mu_i \varphi_{rdi} e_2 \\ \frac{de_3}{dt} = -k_3 e_3 + a_i R_{ri} L_{mi} e_4 \end{cases} \quad (14)$$

The time derivative of (13) is as:

$$\begin{cases} \frac{de_2}{dt} = \frac{di_{isq}^{ref}}{dt} - \psi_{2i} - \frac{1}{\sigma_i L_{si}} u_{sqi} \\ \frac{de_4}{dt} = \frac{di_{isd}^{ref}}{dt} - \psi_{1i} - \frac{1}{\sigma_i L_{si}} u_{sdi} \end{cases} \quad (15)$$

In (15), the control input Stator voltages u_{sqi} and u_{sdi} appeared. New Lyapunov function based on errors in speed, rotor flux, and stator currents, such that:

$$V_2 = \frac{1}{2} e_1^2 + \frac{1}{2} e_2^2 + \frac{1}{2} e_3^2 + \frac{1}{2} e_4^2 \quad (16)$$

The derivative of (16) is given by:

$$\frac{dV_2}{dt} = \frac{de_1}{dt} e_1 + \frac{de_2}{dt} e_2 + \frac{de_3}{dt} e_3 + \frac{de_4}{dt} e_4 \quad (17)$$

By setting (13) in (17), one can obtain:

$$\begin{aligned} \frac{dV_2}{dt} &= e_1(-k_1 e_1 + \mu_i \varphi_{rdi} e_2) + e_2 \left(\frac{di_{isq}^{ref}}{dt} - \psi_{2i} - \frac{1}{\sigma_i L_{si}} u_{sqi} \right) \\ &+ e_3(-k_3 e_3 + a_i R_{ri} L_{mi} e_4) + e_4 \left(\frac{di_{isd}^{ref}}{dt} - \psi_{1i} - \frac{1}{\sigma_i L_{si}} u_{sdi} \right) \\ &= -k_1 e_1^2 - k_3 e_3^2 - k_1 e_3^2 - k_3 e_4^2 + e_2 \left(\mu_i \varphi_{rdi} e_1 + k_2 e_2 + \frac{di_{isq}^{ref}}{dt} - \psi_{2i} - \frac{1}{\sigma_i L_{si}} u_{sqi} \right) \\ &+ e_4 (a_i R_{ri} L_{mi} e_3 + k_4 e_4 + \frac{di_{isd}^{ref}}{dt} - \psi_{1i} - \frac{1}{\sigma_i L_{si}} u_{sdi}) \end{aligned} \quad (18)$$

The stator voltages are then determined by the inputs as:

$$\begin{cases} u_{sdi} = \sigma_i L_{si} (a_i R_{ri} L_{mi} e_3 + k_4 e_4 + \frac{di_{isd}^{ref}}{dt} - \psi_{1i}) \\ u_{sqi} = \sigma_i L_{si} (\mu_i \varphi_{rdi} e_1 + k_2 e_2 + \frac{di_{isq}^{ref}}{dt} - \psi_{2i}) \end{cases} \quad (19)$$

where K_2 and K_4 are positive parameters chosen to ensure a faster dynamic of the rotor speed, rotor flux, and stator currents. Then (15) can be written as:

$$\begin{cases} \frac{de_2}{dt} = -k_2 e_2 - \mu_i \varphi_{rdi} e_1 \\ \frac{de_4}{dt} = -k_4 e_4 - a_i R_{ri} L_{mi} e_3 \end{cases} \quad (20)$$

This can be rewritten as:

$$\frac{dV_1}{dt} = -k_1 e_1^2 - k_2 e_2^2 - k_3 e_3^2 - k_4 e_4^2 \leq 0 \quad (21)$$

The closed loop error system is expressed as:

$$\begin{bmatrix} \frac{de_1}{dt} \\ \frac{de_3}{dt} \\ \frac{de_2}{dt} \\ \frac{de_4}{dt} \end{bmatrix} = A \cdot \begin{bmatrix} e_1 \\ e_3 \\ e_2 \\ e_4 \end{bmatrix} = \begin{bmatrix} -k_1 & 0 & \mu_i \varphi_{rdi} & 0 \\ 0 & -k_3 & 0 & a_i R_{ri} L_{mi} \\ -\mu_i \varphi_{rdi} & 0 & -k_2 & 0 \\ 0 & -a_i R_{ri} L_{mi} & 0 & -k_4 \end{bmatrix} \cdot \begin{bmatrix} e_1 \\ e_3 \\ e_2 \\ e_4 \end{bmatrix} \quad (22)$$

It is interesting to note that the speed of convergence of the error signals to the reference signals depends on the dynamics of the matrix A in (22), in other words, the values of the gains k_1 , k_2 , k_3 , and k_4 depend on the desired position of the poles in closed loop.

3. SIMULATION RESULTS AND DISCUSSION

Elastic band and two induction motors coupled structures are used to validate, by simulation, the dynamic performances, effectiveness and robustness of the backstepping proposed control strategy in the presence of type A symmetrical voltage dips. These results are compared to PI control that has been presented in [2] and the sliding mode control (SMC) that has been presented in [14], [28]. All parameters are listed in Tables 1 and 2.

The models in Figures 2 and 3 were implemented in the Matlab/Simulink environment. Furthermore, we used models from the "SimPowerSystems" Blockset for induction motors and associated electrical converters, which provides comprehensive models that are close to reality. The system was set to run at a speed of 35 m/s, with a mechanical tension set-point of 4 N for the mechanical tension. The simulation results for the proposed structure system for a two three-phase IM fed by PWM voltage source inverters ($V_{dc}= 281$ V) with a rated speed of 35 m/s were obtained using PI indirect rotor flux-oriented control (PI-IRFOC), (SMC), and (BSC).

Table 1. Rating parameters of MMS

Symbol	Description	Value
S	Enchainment section.	$2 \cdot 10^{-3} \text{ m}^2$
L_b	Enchainment length	2 m
E	Band Young modulus.	$0,2 \cdot 10^9 \text{ N/m}^2$
C	DC link capacitor	$1650 \mu\text{F}$
L	DC link inductance	$115 \mu\text{H}$
L_{si}	Stator inductance	80,6 mH
L_{ri}	Rotor inductance	80,6 mH
L_{mi}	Mutual inductance	77,4 mH
R_{si}	Stator resistance	$0,7 \Omega$
R_{ri}	Rotor resistance	$0,31 \Omega$
J_i	Inertia factor	$0,0357 \text{ kg.m}^2$
f_i	Viscous friction factor	$0,003 \text{ N.m.s}$
V_s	voltage	120/208 V
P	Nominal power	2 kW
N	Nominal speed	1750 rpm
p	Number of pole pairs	2

Table 2. Backstepping control parameters

K_1	K_2	K_3	K_4
600	300	100	50

When there are type A voltage dips at time $t=4$ s, the rectifier bridge blocks, zero DC link current shown in Figure 4, the DC link voltage drops shown in Figure 5, and both motors decelerate at their own rate shown in Figure 6(a). The motors are constrained to maintain similar speeds due to the stress associated with the mechanical link between the motors via elastic band.

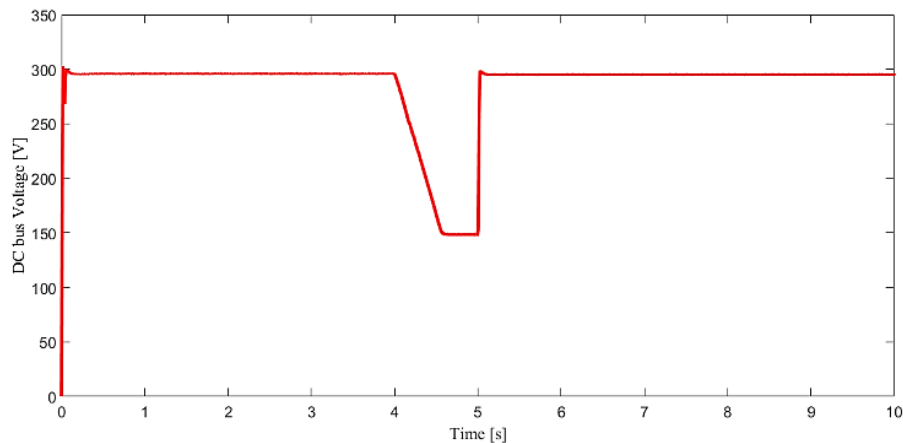


Figure 4. Simulation results for 1 s [4 s 5 s] duration sag response of multi-motors system using BSC, DC-bus voltage behavior

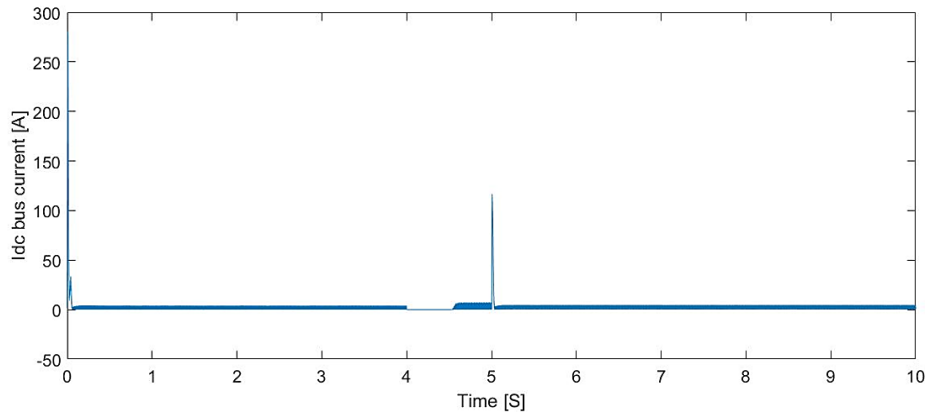


Figure 5. Simulation results for 1 s [4 s 5 s] duration sag response of multi-motors system using BSC, DC-bus current behavior

Following the disappearance of the voltage dip at time $t=5$ s, there is a sudden change in the difference between the voltage available on the network and the voltage on the DC link, resulting in a strong current. This results in a high-current call (overcurrent) that charges the DC link capacity. This will also cause an overvoltage on the DC link due to inductances in the system. When the DC link voltage is restored, both motors can accelerate with a high current draw to the speed set point. Table 3 provides a brief comparison of the various performances obtained from simulation results for the three-control strategy.

The resulting for BSC, PI-IRFOC, and SMC are shown side by side in Figure 6, along with linear speeds and mechanical tension. The performance of the three control methods is compared using various criteria such as dynamic response, stability properties, ease of controller design, and robustness to voltage sags. These criteria are examined individually below:

- Dynamic response: Figure 6 shows the system response; (a) speed evolution using PI-IRFOC, (b) mechanical tension using PI-IRFOC, (c) speed evolution using SMC, (d) mechanical tension using SMC, (e) speed evolution using BSC, and (f) mechanical tension using BSC. In comparison to the PI-IRFOC, SMC and non-linear BSC provide better tracking responses and faster speed response for multi-motor systems. Before and after the voltage sag, the mechanical tension of the material web is maintained constant. Moreover, compared to PI-IRFOC and SMC, BSC has small oscillations during the sag.
- Stability properties: For PI-IRFOC, the stability analysis is performed using a pole placement or full state feedback (FSF) and pole compensation, whereas for BSC and SMC, the Lyapunov stability method is used. It can be seen that all methods have stable performances, but BSC and SMC have faster convergence.
- Robustness to voltage sags: BSC proposed control strategy ensures good voltage dip immunity. In addition, due to a voltage drop at $t=4$ seconds, the DC link voltage has decreased by 50% and remain at this level for 1 second. Figure 6 highlights the impact of the grid voltage dip on the mechanical tension. BSC shown in Figure 6(f) ensures low oscillations on the elastic material compared to SMC shown in Figure 6(d) and PI-IRFOC shown in Figure 6(b).
- Ease of controller's design: The PI-IRFOC is characterized by two parameters. The pole placement technique was used to determine these parameters in a closed-loop. Achievable dynamics are constrained; one obvious limitation is that the poles must be placed on the complex plane's left half to ensure closed loop stability. The dynamic response of the system is improved by BSC and SMC, which are based on a system model. Furthermore, Hurwitz is used to determine the parameters of the BSC controller in closed-loop. Nonetheless, the real parts of the eigenvalues of the previously given matrix A are all negative.

Table 3. comparison of the studied technique

Comparison criteria	BSC	SMC	PI-IRFOC
Dynamic response	good	good	medium
Relative stability	excellent	excellent	high
Robustness to voltage sags	good	medium	medium
Ease of controller design	high	high	high

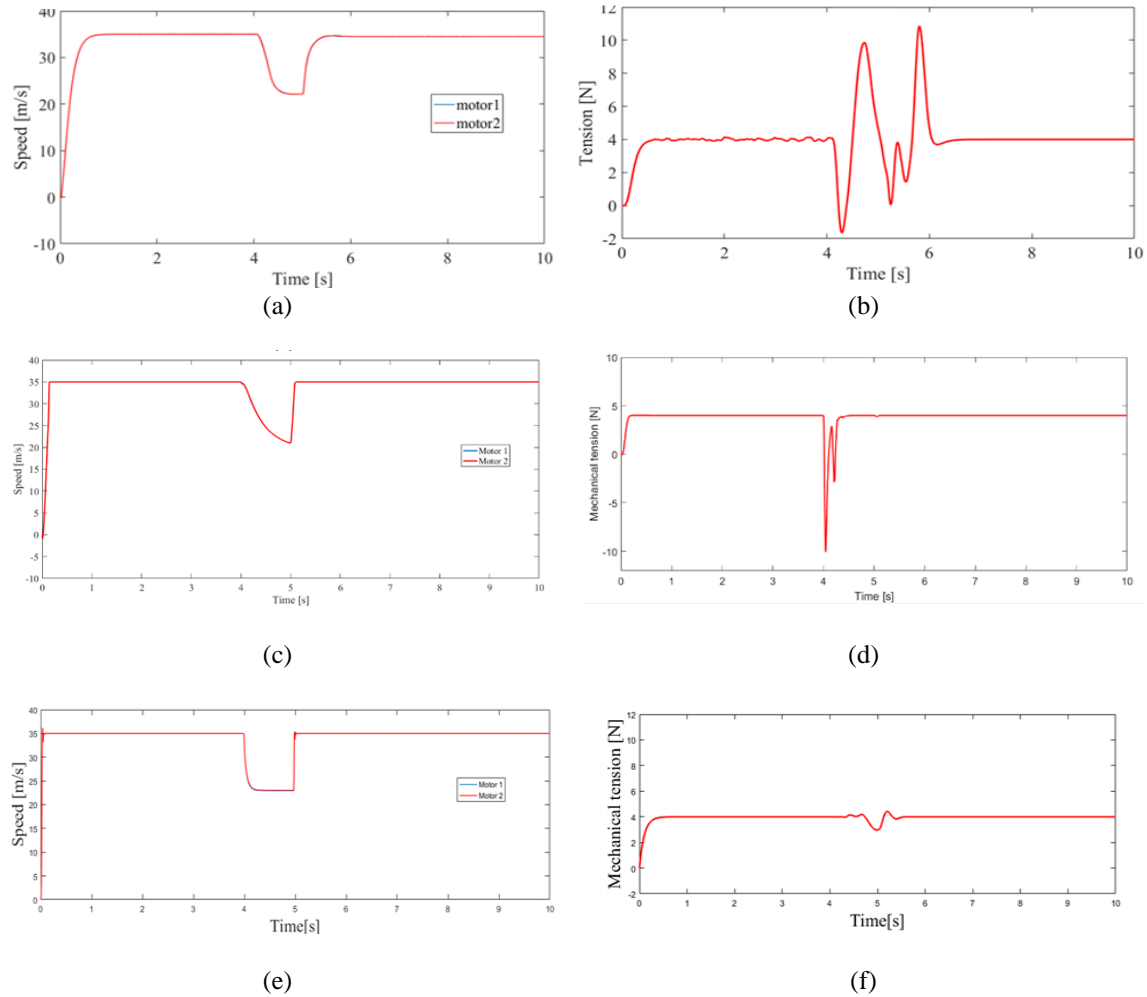


Figure 6. Simulation results for 1 s [4 s 5 s] duration sag response of a multi-motor system, (a) speed evolution using PI-IRFOC, (b) mechanical tension using PI-IRFOC, (c) speed evolution using SMC, (d) mechanical tension using SMC, (e) speed evolution using BSC, (f) mechanical tension using BSC

4. CONCLUSION

In this paper, we compare three control laws for controlling the speed and mechanical tension of a multi-motor system. The investigated system is made up of two induction motors connected by an elastic band. In order to design an improved control law for the linear speed of the web based on the Backstepping strategy, we evaluated the system's behavior in the presence of voltage sags. Simulation was used to assess the effectiveness of the proposed control scheme. This nonlinear control method was compared to existing SMC and PI-IRFOC techniques.




This work allowed us to make a technological contribution to high performance multi-motors systems. Simulation results clearly showed the problems created in drives with variable and coupled speeds/mechanical tension. The advantages of the three investigated control structures are that they compensate the effects of non-linearity and voltage dips and that they ensure a good internal stability of the system. The obtained results confirm the proposed Backstepping control strategy's high performance in terms of rise time, faster transient response, and robustness to voltage sags when compared to SMC and PI-IRFOC. Note that the mechanical tension oscillations observed at start-up with the Backstepping control law are due to the excitation of the system by discontinuous set-points (step) and the presence of derivatives blocs in the controller. These oscillations could be significantly damped by filtering the set-points. For future works, we are planning to develop a multi-motors system management strategy to mitigate other types of voltage sags.

REFERENCES




- [1] G. Scelba *et al.*, "Current-Sharing Strategies for Fault-Tolerant AC Multidives," *IEEE Trans. Ind. Appl.*, vol. 51, no. 5, pp. 3943–3953, 2015, doi: 10.1109/TIA.2015.2439644.

- [2] X. Chu, X. Nian, M. Sun, H. Wang, and H. Xiong, "Robust observer design for multi-motor web-winding system," *Journal of the Franklin Institute*, vol. 355, no. 12, pp. 5217–5239, 2018, doi: 10.1016/j.jfranklin.2018.05.002.
- [3] P. R. Raul and P. R. Prabhakar, "Design and implementation of adaptive PI control schemes for web tension control in roll-to-roll (R2R) manufacturing," *ISA Transactions*, vol. 56, pp. 276–287, 2015, doi: 10.1016/j.isatra.2014.11.020.
- [4] M. H. J. Bollen, "Understanding Power Quality Problems - Voltage Sags and Interruptions," 1st edition, Wiley-IEEE Press, 2000, doi: 10.1109/9780470546840.
- [5] M. BENSALID, A. BA-RAZZOUK, M. ELHAROUSSI, and B. RACHED, "Effects of Symmetrical Voltage Sags on Two Induction Motors System Coupled with An Elastic Web," *Proceedings of the 2020 IEEE 2nd International Conference on Electronics, Control, Optimization and Computer Science (ICECOCS)*, 2020, pp. 1–6, doi: 10.1109/ICECOCS0124.2020.9314298.
- [6] S. Quaia, F. Tosato, and R. Visintini, "Mitigation of voltage sag effects on sensitive plants: an exemplary case study," *Electric Power Systems Research*, vol. 61, no. 2, pp. 93–99, 2002, doi: 10.1016/S0378-7796(02)00009-3.
- [7] S.W. Wahab and A. M. Yusof, "Voltage Sag and Mitigation Using Dynamic Voltage Restorer (DVR) System," *Elektrika*, vol. 8, no. 2, pp. 32–37, 2006.
- [8] K. Somsai, "Controller Design of UPQC for Enhancing Power Quality in Distribution System," *International Journal of Power Electronics and Drive System (IJPEDS)*, vol. 9, no. 4, pp. 1591–1606, Dec 2018, doi: 10.11591/ijpeds.v9.i4.pp1591-1606.
- [9] B. B. Ambati, V. Khadkikar, "Optimal Sizing of UPQC Considering VA Loading and Maximum Utilization of Power-Electronic Converters," *IEEE Trans. On Power Delivery*, vol. 29, no. 3, pp. 1490–1498, June 2014, doi: 10.1109/TPWRD.2013.2295857.
- [10] F. A. Abdulmunem and A. M. Obais, "Design of a continuously and linearly controlled VSI-based STATCOM for load current balancing purpose," *International Journal of Power Electronics and Drive System (IJPEDS)*, vol. 12, no. 1, pp. 183–198, 2021, doi.org/10.11591/ijpeds.v12.i1.pp183-198.
- [11] A. Benali, M. Khiat and M. Denai, "Voltage profile and power quality improvement in photovoltaic farms integrated medium voltage grid using dynamic voltage restorer," *International Journal of Power Electronics and Drive System (IJPEDS)*, vol. 11, no. 3, pp. 1481–1490, 2020, doi.org/10.11591/ijpeds.v11.i3.pp1481-1490.
- [12] C. Kumar and M. K. Mishra, "A Voltage-Controlled DSTATCOM for Power-Quality Improvement," *IEEE Trans. On Power Delivery*, vol. 29, no. 3, pp. 1499–1507, 2014, doi: 10.1109/TPWRD.2014.2310234.
- [13] J. Y. Zhang *et al.*, "Electric Energy Exchange and Applications of Superconducting Magnet in an SMES Device," *IEEE Trans. on Applied Superconductivity*, vol. 24, no. 3, pp. 1–7, 2014, doi: 10.1109/TASC.2013.2291438.
- [14] P. T. Thanh, T. X. Tinh, D. P. Nam, D. S. Luat, and N. H. Quang, "On finite-time output feedback sliding mode control of an elastic multi-motor system," *International Journal of Power Electronics and Drive System (IJPEDS)*, vol. 12, no. 1, pp. 10–19, 2021, doi: 10.11591/ijpeds.v12.i1.pp10-19.
- [15] R. K. Saravanakumar, K. V. Kumar, and K. K. Ray, "Sliding mode control of induction motor using simulation approach," *International Journal of Computer Science and Network Security*, vol. 9, no. 10, pp. 93–104, 2009.
- [16] D.-I. Kim, I.-J. Ha, and M.-S. Ko, "Control of induction motors via feedback linearization with input–output decoupling," *International Journal of Control*, vol. 51, no. 4, pp. 863–883, 1990, doi: 10.1080/00207179008934102.
- [17] R. Salim, A. Mansouri, A. Bendiabdellah, S. Chekroun, and M. Touam, "Sensorless passivity-based control for induction motor via an adaptive observer," *ISA Transactions*, vol. 84, pp. 118–127, 2018, doi: 10.1016/j.isatra.2018.10.002.
- [18] A. Zaafour, C. B. Regaya, H. B. Azza, and A. Châari, "DSP-based adaptive backstepping using the tracking errors for high-performance sensorless speed control of induction motor drive," *ISA Trans.*, vol. 60, pp. 333–347, 2016, doi: 10.1016/j.isatra.2015.11.021.
- [19] J.-J. Wang and J. He, "Torque and flux direct backstepping control of induction motor," *Seventh World Congress on Intelligent Control and Automation*, Chongqing, 2008, pp. 6407–6410, doi: 10.1109/WCICA.2008.4593898.
- [20] D. Knittel, E. Laroche, D. Gigan, and H. Koç, "Tension control for winding systems with a two degrees of freedom H_∞ controller," *IEEE Trans. on Industry Applications*, vol. 39, no. 1, pp. 113–120, 2003. DOI: 10.1109/TIA.2002.807231.
- [21] A. Benlatreche, D. Knittel, and E. Ostertag, "State feedback control with full or partial integral action for large scale winding systems," *40th IAS Annual General Meeting. Conf. Record of the 2005 Industry Applications Conf.*, vol. 2, 2005, pp. 973–978, doi:10.1109/IAS.2005.1518469.
- [22] M. Elhaissof, E. Lotfi, B. Rached, M. Elharoussi, and A. Ba-Razzouk, "DSP Implementation in the Loop of the Indirect Rotor Field Orientation control for the Three-Phase Asynchronous Machine," in *Proceedings of the 2nd International Conference on Computing and Wireless Communication Systems - ICCWCS'17*, no. 52, pp. 1–7, 2017, doi:10.1145/3167486.3167541.
- [23] M. Bensaid, B. Rached, M. Elharoussi, and A. Barazzouk, "Multi-drive electric vehicle system control using backstepping strategy," *Proceedings of the 1st International Conference on Innovative Research in Applied Science, Engineering and Technology (IRASET)*, 2020, pp. 1–6, doi:10.1109/IRASET48871.2020.9092164.
- [24] A. BA-RAZZOUK, A. CHERITI, and P. SICARD, "Implementation of a DSP based real-time estimator of induction motors rotor time constant," *IEEE Transactions on Power Electronics*, vol. 17, no. 4, pp. 534–542, July 2002, doi:10.1109/TPEL.2002.800963.
- [25] A. BA-RAZZOUK, A. CHERITI, G. OLIVIER, and P. SICARD, "Field-oriented control of induction motors using neural-networks decouplers," *IEEE Transactions on Power Electronics*, vol. 12, no. 4, pp. 752–763, July 1997, doi:10.1109/63.602571.
- [26] H. Koç, D. Knittel, M. de Mathelin, and G. Abba, "Modeling and robust control of winding systems for elastic webs," *IEEE Trans. on Control Systems Technology*, vol. 10, no. 2, pp. 197–208, 2002, doi: 10.1109/87.987065.
- [27] V. T. Ha, L. T. Tan, N. D. Nam, and N. P. Quang, "Backstepping control of two-mass system using induction motor drive fed by voltage source inverter with ideal control performance of stator current," *International Journal of Power Electronics and Drive System (IJPEDS)*, vol. 10, no. 2, pp. 720–730, June 2019, doi: 10.11591/ijpeds.v10.i2.pp720-730.
- [28] H. Glaoui, A. Hazzab, B. Bouchiba, I. K. Bousserhane, and P. Sicard, "Fuzzy Sliding-Mode Control for a five drive web-winding System," *International Journal on Electrical Engineering and Informatics*, vol. 3, no 1, pp. 83–99, March 2011, doi: 10.15676/ijeei.2011.3.1.7.




BIOGRAPHIES OF AUTHORS

Bensaïd Mounir    was born in Ouazzane, Morocco. He is a PhD student in the Laboratory Mathematics, Computer and Engineering Sciences Laboratory (MISI), Team: Systems Analysis and Information Processing (ASTI), FST Settat, Hassan 1st University, Morocco. He received the Master in Automatic, Signal Processing and Industrial Computing from Science and Technical Faculty, Hassan 1st University, Settat, Morocco in 2018. His research consists in Modeling, characterization, control and optimization of multi- drive systems. He can be contacted at email: mo.bensaid@uhp.ac.ma.






Abdellfattah Ba-Razzouk    received the Master's degree (M.Sc.A.) in industrial electronics from the Université du Québec à Trois-Rivières (UQTR), Quebec, Canada, in 1993, and the Ph.D. degree in electrical and computer engineering from the École Polytechnique de Montréal, Quebec, Canada, in 1998. From 1997 to 2003, he was a Lecturer in “motors modelling and control” at the Department of Electrical and Computer Engineering, UQTR. In September 1998, he joined the Hydro-Quebec Industrial Research Chair on Power and Electrical Energy, UQTR, where he has been a Professional Research Scientist working on “high-performance intelligent control of electrical drives”. Since June 2009, he is a professor in electrical engineering with the Department of Applied Physics and a Researcher affiliated to “Systems Analysis and Information Processing Laboratory”, both at the Faculté des Sciences et Techniques, Université Hassan 1er of Settat, Morocco. His research interests include high performance control of adjustable speed drives, parameter identification and adaptive control of electrical motors, neural networks, real-time embedded control systems, renewable energy systems, modelling and computer aided design, and real-time simulation of power electronics systems using multiprocessors platforms. He can be contacted at email: barazzou@yahoo.ca.



Mustapha Elharoussi    was born in Azilal Morocco in 1974; he received his PhD in Error Correcting Codes from Mohammed V University Morocco in 2013. In 2014 he joined, as Professor, applied Physics department of FST, Hassan 1st University, Settat, Morocco. He can be contacted at email: m.elharoussi@gmail.com.



Bouchaib Rached    received his PhD in Electrical Engineering “Automatic, Electrotechnics and Electronics” in 2022 from FST Settat, Hassan 1st University, Morocco. He received an engineer's degree in Electrical Engineering from Mohammadia School of Engineering Morocco in 2012. His research activities include the design and implementation in digital calculator of advanced control algorithms of a wind energy system based on the Doubly Fed Induction Generator connected to the grid. He also has research interests ranging from signal processing to industrial application of Automatic Control. He can be contacted at email: bouchaib.rached@gmail.com.